ORIGINAL PAPER

On the enhancement of bond toughness for Al/epoxy T-peel joints with laser treated substrates

**Marco Alfano · Gilles Lubineau ·
Franco Furgiuele · Glaucio H. Paulino**

Abstract   The aim of the present work is to quantify the enhancement of bond toughness of Al/epoxy joints associated to substrates laser irradiation. For this reason a potential based cohesive model is employed and cohesive elements are implemented within the finite element framework. The influence of the cohesive properties on the predicted global response of the joints is firstly analyzed. The coupling between adherents plasticity and the cohesive properties is then discussed. It is shown that the global response is mainly affected by cohesive energy (the bond toughness) and cohesive strength. In turn, a proper cost function is defined which quantifies the deviation between numerical and experimental total dissipated energy. Based on a sensitivity analysis of the as-defined cost function, it is shown that an accurate estimation of the bond toughness can be expected from global data. The situation is different for the cohesive strength, whose estimation could require more advanced experimental observations or additional tests. The results reported in the present work allow us to conclude, in a reliable manner, that the laser surface treatment can lead to a large improvement of bond toughness.

1 Introduction

The design of multi-material structures in automotive and aviation industries led to the need of bonding together dissimilar materials in a fast and efficient way. From this point of view, adhesive bonding provides many advantages over traditional joining techniques. For instance, it reduces the risk of galvanic coupling and increases fatigue life (Adams et al. 1997; Kinloch 1987). However, the mechanical behavior of the joint heavily depends on the adhesion at the adhesive/substrate interface; indeed the occurrence of delamination and/or debonding is critical to the overall integrity of built-up structures. As a consequence, one of the most important step in the design and fabrication of adhesive bonds is the selection or development of suitable surface preparation techniques (Adams et al. 1997; Kinloch 1987; Baldan 2004).

Recent works carried out on this subject have shown that laser irradiation of sample substrates is a suitable alternative to classical mechanical and chemical

M. Alfano (✉) · G. Lubineau
COHMAS Laboratory, Division of Physical Science
and Engineering, King Abdullah University of Science
and Technology (KAUST), Thuwal 23955-6900,
Kingdom of Saudi Arabia
e-mail: marco.alfano@kaust.edu.sa

F. Furgiuele
Department of Mechanical Engineering,
University of Calabria, Via P. Bucci 44C, 87036 Rende,
Cosenza, Italy

G. H. Paulino
Department of Civil and Environmental Engineering,
University of Illinois at Urbana-Champaign,
205 N. Matthew Avenue, Urbana, IL, 61801, USA

treatments (Man and Zhao 2006; Baburaj et al. 2007; Belcher et al. 2010; Rechner et al. 2010; Alfano et al. 2011a,b, submitted). It allows to increase the joint strength thanks to improved mechanical interlocking (Man and Zhao 2006; Baburaj et al. 2007), enhanced substrates wetting (Belcher et al. 2010; Alfano et al. submitted) and to the effective removal of surface weak boundary layers (Rechner et al. 2010; Alfano et al. 2011a,b). The effectiveness of surface treatments in previous works was often qualified by means of the apparent average shear stress[1] determined using standard single lap joints. This is a somewhat qualitative information, and while current design procedures are not solely based on strength but also on damage and fracture resistance, none of the previous work investigated the variation of bond toughness induced by the laser process.

In a companion paper we reported about the effect of Yb-fiber laser substrate irradiation on the strength of Al/epoxy T-peel joints (Alfano et al. submitted). The T-peel test is listed among the ASTM standards available for adhesive joints (ASTM 2008). It resembles actual geometries and stresses likely to be encountered in service conditions and enables the assessment of new adhesive formulations or surface preparation techniques (Adams et al. 1997; Kinloch 1987). Moreover, the T-peel joint is of simple and inexpensive fabrication. The laser surface treatment carried out in Alfano et al. (submitted) promoted mechanical interlocking and an increase in strength so that final failure of the T-peel joint always occurred in conjunction with large substrates plastic deformations[2] Alfano et al. (submitted). It has been observed in previous related works that the occurrence of plastic dissipation may limit considerably the application of the peel test to the assessment of the mechanical behavior of adhesive joints (Kinloch et al. 1994; Wei and Hutchinson 1998; Wei 2002). In fact, if the condition for linear elastic fracture mechanics are satisfied, then the steady state peel force per unit width, which is related to the macroscopic work of fracture, would effectively represent the bond toughness of the joint. However, for thinner substrates, such as those employed for the T-peel test reported in Alfano et al. (submitted), plastic deformations do occur before

fracture and affect the amount of external work which is effectively available for the debonding process. As a result the peel force does not solely represent the work of adhesion, but it also embeds the plastic dissipation. A partition between the two contributions would allow us to infer the bond toughness. Earlier attempts in this direction were made using beam bending analysis (Kinloch et al. 1994). However, later work showed that using this approach essential features of the debonding process are lost (Wei and Hutchinson 1998; Wei 2002; Yang et al. 2000) and that accurate interpretation of experimental data could be achieved using the cohesive zone model of fracture (CZM) (Dugdale 1960; Barenblatt 1962).

The aim of the present work is to complement the results of our previous study (Alfano et al. submitted) by means of an extensive series of numerical simulations carried out using the CZM. The objective is to identify the increase in bond toughness provided by the laser process. The CZM lends itself to the analysis of plastically deforming adhesive joints because it allows to separate the energy needed to propagate the crack from that dissipated through the plastic deformation of the bonded substrates. The CZM has been already applied with success to the analysis of adhesive joints failing with large plastic deformations under mode I (Yang et al. 1999, 2000; Kafkalidis et al. 2000), mode II (Yang et al. 2001) and mixed mode (Yang and Thouless 2001) loading conditions. In particular, in the present paper, the Park-Paulino-Roesler (PPR) (Park et al. 2009) potential based cohesive model is employed and cohesive elements are implemented in a FE commercial code (ABAQUS/Standard). In the case of mode-I fracture the parameters of the PPR are the cohesive strength (σ_{max}), the cohesive energy (ϕ_n), the shape parameter (α) and the slope indicator (λ_n). A sensitivity around the influence of these parameters on the predicted peel-force versus displacement plots is firstly carried out. The results are presented as a function of non-dimensional groups obtained from a standard dimensional analysis. Afterwards, the coupling between fracture and macroscopic adherents plasticity is discussed. It is shown that the global response (i.e. the load-displacement curve) is mainly affected by cohesive energy and cohesive strength. In turn, these parameters are obtained comparing experiments and simulations. In particular, a cost function is defined which quantifies the difference between numerical and experimental load-displacement curves. In such way

---

[1] The ratio between the failure load and the nominal bonding area.

[2] Localized near the crack tip and in the L-bend regions of sample substrates.

the combination of cohesive properties providing a reasonable match between experiments and simulations for the problem at hand is estimated.

This paper is organized as follows. Section 2 summarizes the experimental results. In Sect. 3 a theoretical background on the PPR model and details on the implementation of interface elements in the FE framework are reported. Section 4 is then concerned with the sensitivity analysis and the identification of bond toughness. Finally, in Sect. 5 final remarks are provided to end the paper.

2 Experimental section

Laser irradiation of samples surface has been carried out using an ytterbium fiber laser operated in pulsed mode (IPG, YLP1-100-100). An experimental study on the effect of process parameters on the resulting wettability of substrate surfaces has been already described in detail elsewhere (Alfano et al. submitted). Here we summarize the key conclusions at the light of some additional information. In order to set suitable processing conditions different technological parameters were investigated, e.g. average power (P), laser velocity (v) and line spacing (LS). This choice was motivated by the need to identify a combination ensuring improved wetting of the solid substrates and fast processing at the same time. Performing systematic fracture tests was obviously unpractical, because of the high number of configurations to investigate. Thus, measuring the wettability through the variation of contact angle was chosen as a quick way to benchmark the quality achieved for a specific set of process parameters. The contact angle can be very informative in order to assess the cleanliness of solid surface and to qualify the effectiveness of a surface pre-treatment (Adams et al. 1997). The contact angle was determined using an optical contact meter using glycerol as testing liquid. It was firstly observed that laser power levels below 100 W were not able to improve wetting (i.e. decrease the contact angle) and failed to provide a surface morphology prone to mechanical interlocking. Therefore the power level was set equal to 100 W and attention was subsequently limited to the effect of line spacing and laser speed. The results reported in Fig. 1 show that the laser process allows to decrease contact angle with respect to both as-produced and grit-blasted conditions. The bars denote the variation of contact angle recorded in two
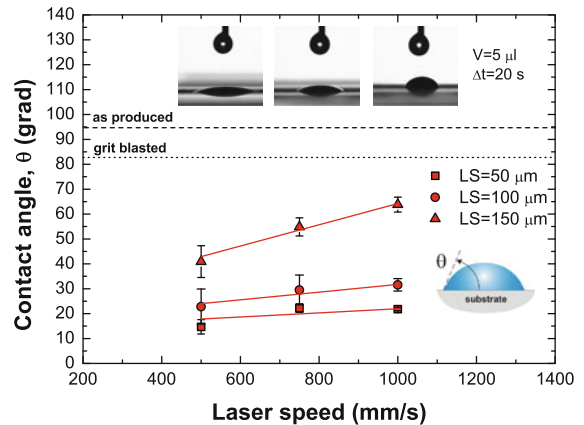
Fig. 1 Variation of contact angle as a function of laser spacing and speed. The *error bars* are referred to the difference recorded in the contact angle observing the liquid drop in the directions *parallel* and *perpendicular* to the processing direction. The *insets* show the glycerol drop resting on treated surfaces obtained for increasing laser speed and at the higher spacing. *V* denotes the volume of the glycerol drop and Δt is the time window employed to observe the evolution of contact angle

orthogonal directions.[3] For the investigated combinations of the process parameters, best results in terms of wetting were obtained for line spacings lower than $150\,\mu m$. Below this value the results slightly depended on process parameters. For the subsequent mechanical tests, the combination of $P = 100\,W$, $LS = 50\,\mu m$ and $v = 750\,mm/s$ was selected.

The mechanical tests were carried out using symmetrical T-peel joints with AA6082T6 sheet metal substrates (thickness $h = 1.5\,mm$, width $B = 25\,mm$) bonded with an epoxy adhesive (Loctite Hysol 9466), whose properties are reported in Loctite Hysol 9466 (2006). The thickness of the adhesive layer was set to $h_a = 0.25\,mm$ using metallic spacers. The metal substrates were bent at 90° before bonding and the bent portions had a length $L = 100\,mm$. An initial pre-crack was introduced using thin teflon sheets. The top parts of the samples ($\ell = 40\,mm$) were held in the grips of a tensile testing machine, and the peel-force versus crosshead displacement curves were recorded as the specimen were broken under quasi static loading conditions. In particular, the results of the mechanical tests are reported in Fig. 2. A remarkable increase in maximum

---

[3] It is emphasized that for some combinations of the process parameters a *patterned* surface was obtained and as a consequence the shape of the liquid drop was elongated in the lasing direction.
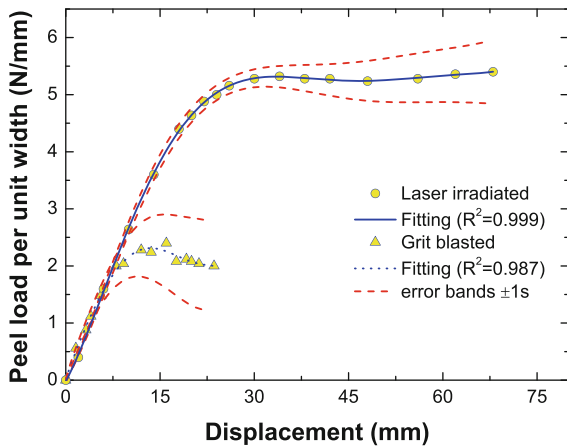
Fig. 2 Experimental load-displacement curves for grit blasted and laser treated samples. The *dashed lines* represent the error bands at $\pm 1 s$ (s: standard deviation). The continuos and the *dotted line* represent the fitting curves of experimental results for laser treated and grit blasted samples, respectively

peel load (and elongation at failure) with respect to standard grit blasting was recorded. The greater scatter observed for grit blasted samples can be addressed to the lower reproducibility of this surface preparation technique. Note that the error bands were determined considering the average of five consecutive measurements. Gross substrate plastic deformations occurred before final failure in the laser treated samples. These were localized around the crack tip and in the L-bend region of the substrates (see Alfano et al. 2011c). For this reason, the peel force is no longer a valid indicator of the strength of the joint (Kinloch et al. 1994; Wei and Hutchinson 1998; Yang et al. 1999, 2000; Wei 2002). Finally, a *transition* from *adhesive* to *cohesive* failure was observed after the laser treatment.

The increase in peel load and the modification of the failure mechanisms testify the improvement in the mechanical behavior of the joint with laser treated substrates. The finite element simulations reported next are therefore aimed to reveal the achieved variation of bond toughness.

3 Analysis of debonding using a potential based cohesive model

3.1 Theoretical background

Finite element simulations of debonding were carried out using cohesive elements implemented in ABAQUS.

The cohesive elements are based on the unified potential for mixed fracture proposed in Park et al. (2009). The potential represents the distribution of fracture energy in conjunction with separation of fracture surfaces. As the present paper deals with a symmetrical 90°-peel test, opening conditions (mode-I) prevails and mixed mode effect can be neglected. In this case, the potential can be simplified

$$\Psi(\Delta_n) = \phi_n + \Gamma_n \left(1 - \frac{\Delta_n}{\delta_n}\right)^\alpha \left(\frac{m}{\alpha} + \frac{\Delta_n}{\delta_n}\right)^m, \quad (1)$$

where Δ_n is the opening displacement, ϕ_n is the mode I cohesive energy, α is the shape parameter and δ_n is the final crack opening width. This last is given by

$$\delta_n = \frac{\phi_n}{\sigma_{max}} \alpha \lambda_n (1 - \lambda_n)^{\alpha-1} \left(\frac{\alpha}{m} + 1\right) \left(\frac{\alpha}{m} \lambda_n + 1\right)^{m-1} \quad (2)$$

where λ_n is the slope indicator and σ_{max} is the cohesive strength. The remaining terms are give as follows, Γ_n is the energy constant

$$\Gamma_n = -\phi_n \left(\frac{\alpha}{m}\right)^m, \quad (3)$$

m the non-dimensional exponent

$$m = \frac{\alpha(\alpha - 1)\lambda_n^2}{(1 - \alpha\lambda_n^2)}, \quad (4)$$

The intrinsic cohesive zone model for the normal cohesive stress, σ_n, is obtained from Eq. 1 as follows

$$\sigma_n = \frac{\partial \Psi}{\partial \Delta_n} = \frac{\phi_n}{\delta_n} \left(\frac{\alpha}{m}\right)^m \left(1 - \frac{\Delta_n}{\delta_n}\right)^{\alpha-1}$$
$$\times \left(\frac{m}{\alpha} + \frac{\Delta_n}{\delta_n}\right)^{m-1} (\alpha + m) \frac{\Delta_n}{\delta_n}, \quad (5)$$

Therefore there are four independent unknown parameters which need to be determined in order to fully define the cohesive interaction (σ_n), i.e. ϕ_n, σ_{max}, λ_n, α. In Fig. 3 the cohesive interaction, σ_n, is plotted for various sets of cohesive parameters; in general, at first increases, when $\Delta_n = \delta_{nc}$ it reaches a maximum (i.e. the cohesive strength, σ_{max}), then it softens and falls to zero when the opening displacement reaches the final crack opening width (δ_n). The so described evolution of σ_n with δ_n is also schematically depicted in the inset of Fig. 3. It is emphasized that the softening curve depends on the chosen value of the shape parameter (α).
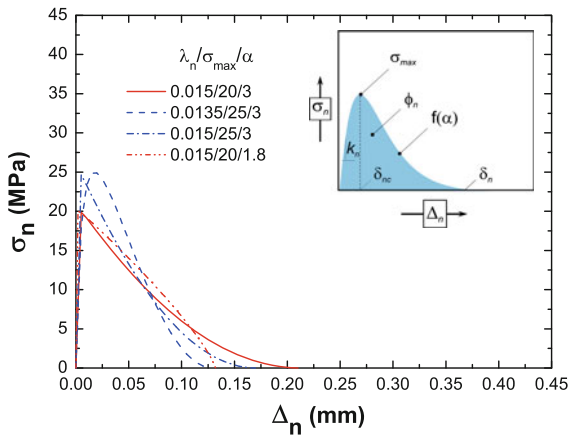
Fig. 3 PPR based intrinsic cohesive relation of normal debonding for various combinations of fracture parameters ($\phi_n = 1.5$ N/mm, σ_{max} is expressed in [MPa]). The *inset* is a schematic depiction of the intrinsic traction separation relation which illustrates the meaning of the cohesive parameters

3.2 Implementation of cohesive elements and development of the FE model

Similarly to previous related works (Yang et al. 1999; Högberg 2006; Alfano et al. 2009, 2011d), in the present paper it is assumed that the role of the adhesive layer is to provide a traction-separation relation across the interface between the two adherents. Therefore the development of a finite element model of the T-peel joint requires cohesive elements for modeling crack initiation, evolution and final failure and continuum elements for the surrounding bulk material. The cohesive elements are herein formulated exploiting the principle of virtual works. The internal work done by the virtual strain ($\delta\epsilon$) in the domain (Ω) and the virtual crack opening displacement ($\delta\Delta$) along the crack line (Σ_c) is equal to the external work done by the virtual displacement (δu) at the traction boundary (Σ), it follows

$$\int_{\Omega} \delta\epsilon^T \sigma \, d\Omega + \int_{\Sigma_c} \delta\Delta^T \mathbf{T} \, d\Sigma_c = \int_{\Sigma} \delta u^T \mathbf{P} \, d\Sigma, \quad (6)$$

where $\mathbf{T}$ is the traction vector along the cohesive zone and $\mathbf{P}$ is the external traction vector. The crack face opening is interpolated by means of standard shape functions, i.e.

$$\left[\int_{\Omega} \mathbf{B}^T \mathbf{E} \mathbf{B} \, d\Omega - \int_{\Sigma_c} \mathbf{N}_c^T \frac{\partial \mathbf{T}}{\partial \Delta} \mathbf{N}_c \, d\Sigma_c \right] \mathbf{d} = \int_{\Sigma} \mathbf{N}^T \mathbf{P} \, d\Sigma, \quad (7)$$

where $\mathbf{N}$ and $\mathbf{N}_c$ are matrices of shape functions for bulk and cohesive elements, respectively; $\mathbf{B}$ is the derivative of $\mathbf{N}$; $\mathbf{d}$ are nodal displacements and $\mathbf{E}$ is the material tangential stiffness matrix for the bulk elements. These integrals are numerically evaluated by a classical Gauss-quadrature rule. Finally, $\frac{\partial \mathbf{T}}{\partial \Delta}$ is the jacobian stiffness matrix, which is given as

$$\frac{\partial \mathbf{T}}{\partial \Delta} = \begin{vmatrix} \frac{\partial T_t}{\partial \Delta_t} & 0 \\ 0 & \frac{\partial T_n}{\partial \Delta_n} \end{vmatrix}. \quad (8)$$

Note that the traction T_n is equivalent to the cohesive interaction for normal de-bonding (σ_n) introduced previously, while T_t is corresponding value in the tangential direction, which however does not enter our calculations. The stiffness matrix and load vector of the cohesive elements are assembled in a user-defined subroutine within the commercial FE code ABAQUS. In the FE model the whole adhesive layer was replaced by a single row of cohesive elements with a finite thickness equal to the nominal adhesive layer thickness. As a consequence the macroscopic constitutive behavior of the layer is expressed as a function of the opening displacement Δ_n and is captured through the cohesive interaction σ_n derived using the PPR potential.[4] The area under the traction-separation relation mimics the energy dissipated within the adhesive layer and represents the bond toughness of the joints.

The size of cohesive elements was chosen observing that for element sizes ≤ 0.1 mm the total dissipated fracture energy (area under the global load-displacement curve) was mesh independent. Therefore, element size was set equal to 0.1 mm throughout the numerical simulations.

For the sample substrates four-nodes continuum elements were employed and plane-strain and large displacement conditions were considered. As noted previously, extensive plastic deformations were recorded during the experiments, for this reason the stress-strain

---

[4] This is a simplified kinematics which only accounts for constant peel and shear deformations through the thickness of the layer (Fedele et al. 2009).

curve of the aluminum alloy was employed as input for the numerical simulations. The uniaxial stress-strain curve was modeled by a piece-wise representation of the experimental data obtained during testing (Alfano 2010). The tensile behavior was generalized to multiaxial stress states assuming isotropic hardening and using the von Mises yield surface. However, it should be noted that J_2 flow theory provides satisfactory results when the cohesive strength does not largely overcome the yielding strength. When $\sigma_y/\sigma_{max} \approx 4 \div 6$ the conventional plasticity theory does not give rise to sufficient stress elevation at crack tip to produce decohesion. In such cases the strain gradient theory of plasticity has been recommended (Wei and Hutchinson 1998; Wei 2002).

4 Determination of the bond toughness of the joint

4.1 Global versus local approaches

An analysis of the literature reveals that there are two viable routes available for the determination of cohesive parameters which can be roughly grouped in *global* and *local* approaches. Global approaches allow to identify the cohesive properties by iteratively adjusting finite element predictions, e.g. load-displacement curves, deflections and/or deformed shape of the sample, to the corresponding experimental quantities (Yang et al. 1999, 2000, 2001; Kafkalidis et al. 2000; Yang and Thouless 2001; Gustafson and Waas 2009). Local approaches are based on a similar inverse procedure, however, the experimental input data are now represented by point values (Ji et al. 2010), or full field sets (Fedele et al. 2009; Shen and Paulino 2011), of surface opening displacement taken in the near crack tip region. Using local approaches information on the precise shape of the traction separation law can be obtained. Such knowledge can be of critical importance, for instance, in order to design tough adhesives. In this case a weak phase (e.g. rubber particles) is introduced to trigger damage development and induce an intrinsic toughening effect (Cavalli and Thouless 2001). Therefore, a detailed knowledge of the cohesive model may help to assess the variation of the final opening displacement in the process zone as a function of the content of the weak phase.

Although it is important from a fundamental prospective, a detailed knowledge of the cohesive model may not always be necessary for predictive modeling of plastically deforming adhesive joints. For instance in the work by Yang et al. (1999), the cohesive energy and the cohesive strength for an adhesive layer were determined from the analysis of residual radius of curvature of plastically deforming wedge-loaded DCB. The so obtained parameters were employed without any modification to successfully predict the experimentally observed load-displacement curve of T-peel samples made up with same materials and with nominally identical bond-line. It was stated that for the prediction of macroscopic load-displacement curves, or deformed shape of the sample, the cohesive strength and cohesive energy were the only information needed and that the shape of the cohesive model was of secondary importance. Likewise in the present work the identification of cohesive model parameters will be based on global load-displacement data recorded for the T-peel joints and presented in the previous section. In particular the cohesive parameters in the numerical model will be adjusted so that to achieve a match with the experimental quantities. However, we emphasize that it is not the intention of this paper to identify the full set of cohesive parameters; rather, the focus is on the enhancement of bond toughness which follows to the laser surface preparation process. The centerpiece of our identification procedure is a sensitivity analysis aimed to assess the sensitivity on the simulated load-displacement curves to the parameters embedded in the PPR cohesive model.

4.2 Sensitivity analysis

The results of the sensitivity analysis are now presented. The data set employed to the purpose is represented by the load-displacement curves (P-δ) generated using the numerical model with a priori known material parameters. The objective is to understand how the variation of cohesive properties affects the simulated P-δ curves. The analysis has been implemented in ABAQUS/Standard, which has been interfaced with Matlab (The Mathworks, Inc.). We firstly note that in our previous study (Alfano et al. 2011c) the effect of different values of α was analyzed and it was concluded that it does not significantly affect the P-δ curve. A similar conclusion concerning the shape of the CZM was also drawn in previous related works which reported about the analysis of crack growth in

elasto-plastic solids (Tvergaard and Hutchinson 1992; Yang et al. 1999). For this reason, in the following numerical simulations the shape parameter was set equal to $\alpha = 3$. However, it is recognized that the shape of the cohesive model may play a role, for instance when the substrates deformation is dominated by linear elasticity, as shown in Alfano et al. (2009), Alfano (2006).

In our modeling approach the stiffness of the adhesive layer is captured by the stiffness of the cohesive model (k_n). In the PPR model the elastic behavior can be controlled by the slope indicator, which is given by $\lambda_n = \delta_{nc}/\delta_n$ (cfr. Fig. 3). At the initial stage of loading the normal separation is very small, and the cohesive relation provided by Eq. 5 can be linearized in term of Δ_n; therefore the stiffness of the cohesive model can be calculated as follows

$$\sigma_n = \frac{\partial^2 \Psi}{\partial \Delta_n^2} \cdot \Delta_n = \left[\frac{\phi_n}{\delta_n^2} \left(\frac{\alpha}{m} \right)^{m+1} \left(\frac{m}{\alpha} \right)^m (m + \alpha) \right]$$
$$\Delta_n = k_n \Delta_n. \tag{9}$$

It has been observed in Alfano et al. (2011c), and also during the development of the present work, that a wide variation[5] of the slope indicator, and then of k_n, does not affect the initial slope of the simulated load displacement curve (i.e. the macroscopic stiffness of the joint). Then, in the subsequent numerical simulations, the slope indicator has been set equal to $\lambda_n = 0.06$. The remaining unknown cohesive parameters are the cohesive strength and the fracture energy. A sensitivity analysis has been carried out in order to assess their effect on the predicted P-δ curve. The dimensionless peel force per unit width of the sample ($\bar{P} = P/B$) can be expressed as a function of the following dimensionless parameters

$$\frac{\bar{P}}{\sigma_y h} = f \left(\frac{\delta}{h}, \underbrace{\frac{\phi_n}{\sigma_y h}, \frac{\sigma_y}{\sigma_{max}}}_{\text{cohesive properties}}, \underbrace{\frac{\sigma_y}{E}, n}_{\text{substrates elasto-plastic properties}} \right), \tag{10}$$

i.e. the opening displacement, cohesive parameters and elasto-plastic properties of the substrates, respectively. Note that E is the Young modulus, σ_y is the yield strength and n is the hardening exponent. These last, as well as the geometrical features of the sample (e.g.

---
[5] Up to two orders of magnitude.
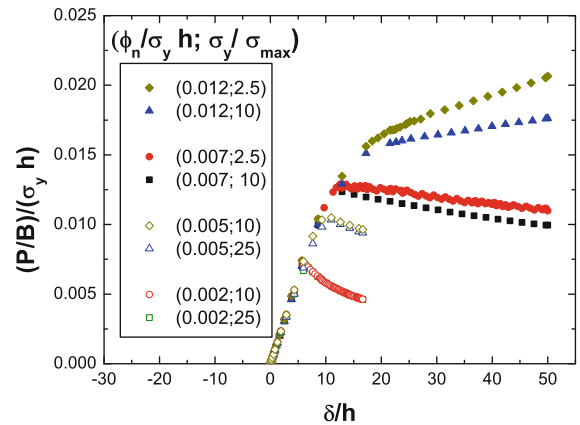
Fig. 4 Sensitivity of the non-dimensional load-displacement curves to cohesive energy and cohesive strength ($\lambda_n = 0.06$ and $\alpha = 3$)

length of the L-bend portion of the sample, the pre-crack-length, etc.), were deliberately excluded from the analyses and regarded as constants and equal to the values reported earlier in the paper. The finite element simulations were carried out in displacement control and the actual ranges of displacements recorded during the experiments were employed. The results of the sensitivity analyses are summarized in Fig. 4. The open symbols are referred to the range of experimental results observed for grit blasted samples. It is inferred that when the fracture energy increases the area under the P-δ curve (global dissipated energy) increases. In addition, for constant fracture energy, a variation of cohesive strength within the chosen range only slight affects the load-displacement curve. Likewise, numerical simulations were carried out in the range of the experimental results pertaining to laser treated samples. We note that the results are pretty sensitive to both σ_{max} and ϕ_n. Indeed, for constant cohesive energy, the slope of the P-δ curve increases with increasing values of cohesive strength. This effect may be addressed to a leveraging effect of plastic deformations in the metal substrates (Tvergaard and Hutchinson 1992; Yang et al. 1999) and it is also in agreement with Yang et al. (2000), where the elevation of the peel force with increasing cohesive strength was illustrated. In summary, the results in terms of P-δ curves are always sensitive to cohesive energy. The sensitivity to σ_{max} increases as the energy increases and is associated to the occurrence of additional plastic dissipation. The interplay between plasticity and cohesive properties is further investigated in the next section.

4.3 On the interplay between cohesive properties and plastic dissipation in the metal substrates

It may be now of interest to quantify the plastic dissipation in the metal substrates as a function of the non-dimensional cohesive parameters. From this standpoint, we note that the total external work w carried out to fracture the sample is given by the sum of the recoverable strain energy (w_e), the total plastic dissipation (w_p) and the total fracture energy (w_f). Therefore, it follows

$$w = w_e + w_p + w_f. \tag{11}$$

The results are shown in Fig. 5, where the ratio w_p/w_e is reported as a function of the dimensionless cohesive strength and fracture energy. The ranges chosen of cohesive parameters match the ones employed in Fig. 4, so that a direct comparison can be made. The results show that in the case of grit blasted samples there is little or no plastic dissipation when the fracture energy is low ($\phi_n/\sigma_y h \approx 0.002$); however, the plastic dissipation increases as the energy increases, although it looks pretty independent of the cohesive strength. On the other hand for laser treated samples, the plastic dissipation is higher and depends on both the cohesive parameters. In this case the plastic dissipation is much sensitive to cohesive energy than to cohesive strength. A comparison among of present results with previous related works is now carried out. In particular, Wei

and Hutchinson (1998), Wei (2002) showed that when plastic deformation does occur the extent to which the peel force (per unit width) excess the work of adhesion is determined by the ratio between the cohesive strength and yielding stress (σ_{max}/σ_y). When this ratio is less than two, plastic dissipation is nearly negligible compared to the bond toughness because the local stress levels around the crack tip are such that there is little or no plastic deformation. On the other hand, plastic dissipation becomes increasingly important when the ratio is larger than 3. However, the results reported in the present work show that extensive plasticity may occur even for low value of the cohesive strength. Indeed, the domain of σ_{max} explored to build Fig. 5 is such that $0.04 \leq \sigma_{max}/\sigma_y \leq 0.4$. Therefore the tractions acting on the substrates within the process zone are not high enough to induce extensive plastic deformations around the crack tip. This is also confirmed by the numerical simulations, which displayed plastic deformations localized at some distance behind the crack tip[6] and triggered in the metal substrates before crack initiation. In other words, the active plastic zone was located behind the advancing crack tip. Interestingly, Yang et al. (1999, 2000) reported essentially a similar conclusion in studying crack propagation in adhesive bonded thin metal sheets, such as those analyzed in this work. An outcome of their study, which is relevant to the present discussion, is that extensive plastic dissipation may occur when $\sigma_{max}/\sigma_y \leq 1$. They stated that the normal tractions acting in the process zone increase the state of triaxiality and make more difficult for yielding to occur, while the substrates deform without applied surface tractions behind the failed cohesive elements. We believe a similar mechanism holds for our simulations. In addition, we observe that in the T-peel joint the dissipation is enhanced because the stress concentration occurring at the L-bend portions of the sample promotes additional plasticity earlier during the test. Moreover, the initial pre-cracked portion of the sample further increases the bending moment acting in the region in proximity of the crack tip and trigger plastic dissipation even before crack initiation. So the plastic dissipation associated to crack growth is related to gross plasticity in the metal substrates.
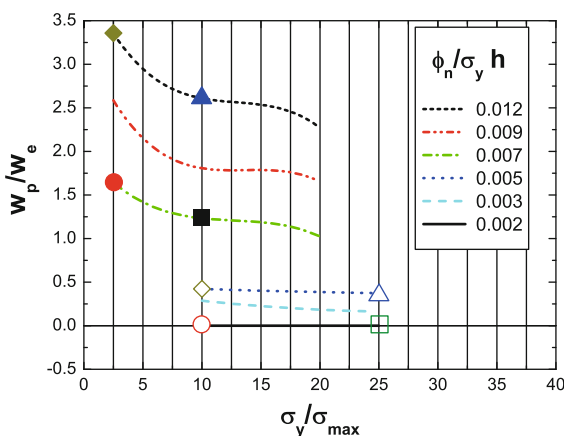
Fig. 5 Plastic dissipation in the metal substrates as a function of cohesive strength (σ_y/σ_{max}) and for different values of the fracture energy ($\phi_n/\sigma_y h$)

---

[6] Especially at the traction free compressive surfaces of the substrates.

4.4 Identification of bond toughness

Based on the results reported in the previous section, the model response determined in terms of global load-displacement curves has a different sensitivity to cohesive energy and cohesive strength. We now want to assess the existence of suitable ranges for these cohesive properties providing best fit with the experimental measurements. To this aim response maps are built to assess wether or not each parameter of the model (ϕ_n and σ_n) can be determined independently for the specific set of experimental data available. Once again we emphasize that our main interest is to gain an understanding on the increase of bond toughness of the joint after the laser process. We may obtain such information looking at the combination of cohesive parameters which allows to achieve a match between experimental and simulated P-δ curves. Specifically, a cost function was built where the difference between experimental and simulated responses is quantified considering the L_2 norm of the total dissipated fracture energy (area under the P-δ curve). In particular

$$\Phi = \|U(\delta_g)_{exp} - U(\delta_g)_{num}\|_2, \tag{12}$$

where

$$U(\delta_g) = \int_0^{\delta_{gf}} P \cdot d\delta_g, \tag{13}$$

and δ_g is the global opening displacement and the subscript gf denotes the final value at which failure (separation of the bonded substrates) was recorded. A simple rectangle quadrature rule has been applied and the experimental energy has been determined considering the polynomial interpolating function of the average of five consecutive displacements. Note that the automatic assignment of parameter values to the FE model was managed interfacing Matlab and ABAQUS by means of a shell script. This choice for the cost function is similar to that made in Gustafson and Waas (2009), Lee et al. (2010). In particular, in Gustafson and Waas (2009) a sensitivity analysis was carried out using the kriging method; the influence of cohesive parameters (cohesive energy, cohesive strength and shape of the model) on the finite element predictions of the maximum load at onset of fracture was analyzed. In Lee et al. (2010) the sensitivity analysis to cohe-

sive properties (cohesive strength and initial stiffness of the model) was carried out considering the whole load-displacement curve. However, it should be pointed out that in these works the effect of substrates plasticity was not accounted for. The ranges of cohesive strength and cohesive energy employed to build our response maps were chosen in such a way to have output load-displacement curves in the range of experimental results.[7] In the case of grit blasted samples the following ranges have been chosen for cohesive strength and cohesive energy: $\phi_n = 0.6 \div 1.2\,\text{N/mm}$, $\sigma_n = 0.25 \div 25\,\text{MPa}$; and for laser treated samples: $\phi_n = 2.5 \div 4.5\,\text{N/mm}$, $\sigma_n = 5 \div 100\,\text{MPa}$. The surface plots of the cost function (Φ/Φ_{max}) are given in Fig. 6 and the corresponding contour plots in Fig. 7. It is apparent that for grit blasted samples combinations of ϕ and σ_{max} minimizing the cost function exist. The values of cohesive strength around which the minimum is located were not included in the range investigated in Figs. 4 and 5. This feature can be also assessed from the analysis of contour plots reported in Fig. 7. It looks that minima values of Φ/Φ_{max} are embedded in the region $\phi_n = 0.7 \div 0.9\,\text{N/mm}$, $\sigma_n = 0.25 \div 5\,\text{MPa}$. The load displacement curve obtained using the average values of cohesive parameters within these intervals is reported in Fig. 8. On the other hand, in the case of laser treated samples a single combination of the cohesive parameters which minimizes the cost function could not be identified. In particular, the minima of Φ/Φ_{max} fall in the following ranges: $\phi_n = 3.2 \div 3.8\,\text{N/mm}$ and $\sigma_{max} = 20 \div 85\,\text{MPa}$. While the range observed for cohesive energy looks reasonably narrow, that of cohesive strength is somewhat wide. As a result, very different values of cohesive strength could lead essentially to the equivalent load-displacement curve. This is also confirmed by the simulated load-displacement curve reported in Fig. 9, which have been obtained using the end-values of the intervals.

5 Discussion and concluding remarks

Previous works showed that the use of σ_{max} and ϕ_n in cohesive models of fracture provides excellent predictive capabilities[8] for plastically deforming adhe-

---

[7] The simulations were carried out in displacement control and the actual end-displacement observed during the experiments was employed.

[8] In terms of global response.
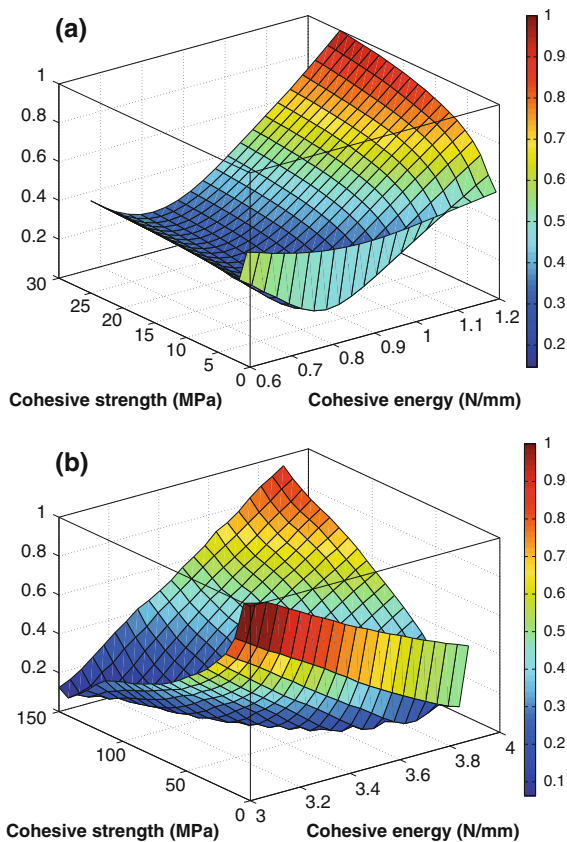
Fig. 6 Surface plots of the cost function $(\frac{\Phi}{\Phi_{max}})$ obtained for samples with **a** grit blasted and **b** laser treated substrates

sive joints (Yang et al. 1999, 2000). However, the results reported in the present work illustrated the low sensitivity of the simulated load-displacement curves of T-peel joints to cohesive strength. A similar issue was also discussed in previous related works (Kafkalidis et al. 2000; Sun et al. 2008). It was clearly pointed out in Sun et al. (2008) that, depending on the specific geometries and materials under examination, the numerical simulations may show low sensitivity to cohesive strength. Those authors showed that cohesive energy of a plastically deforming adhesive joint could be determined comparing numerical and experimental load-displacement curves, while the simulated response was not sensitive to cohesive strength. Therefore an additional test coupon was designed with higher sensitivity to cohesive strength for identification purposes. On the other hand, it was observed in Kafkalidis et al. (2000) that the cohesive strength depends on the constraint level in the joint. Specifically, σ_{max} decreases as the
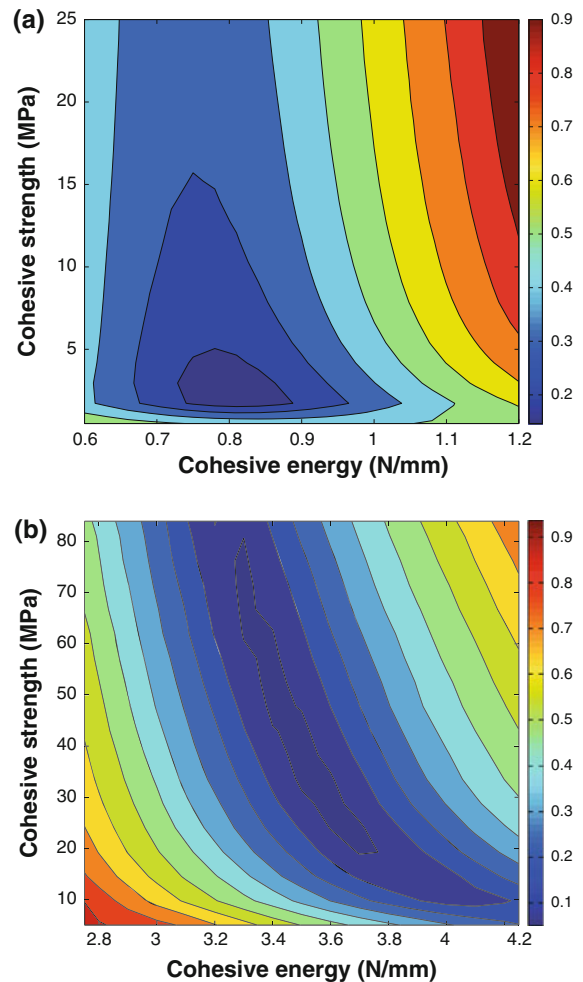
Fig. 7 Contour plots of the cost function $(\frac{\Phi}{\Phi_{max}})$ obtained for samples with **a** grit blasted and **b** laser treated substrates

level of constraint in the joint decreases (i.e. increasing the thickness of the adhesive layer or decreasing the thickness of the adherents) while cohesive energy is relatively unaffected.[9] As a result the analysis of adhesive joint with different constraint levels may require a re-calibration of cohesive strength. For this reason we expect the identified value of bond toughness to be fairly representative of the mode I bond toughness for the present T-peel joints with laser treated substrates. Therefore, on the basis of the previous results, and

---

[9] It was experimentally observed that σ_{max} and δ_n depended on the geometry of the system (substrates and adhesive thicknesses) in such a way that the cohesive energy (ϕ_n) remained approximately constant.
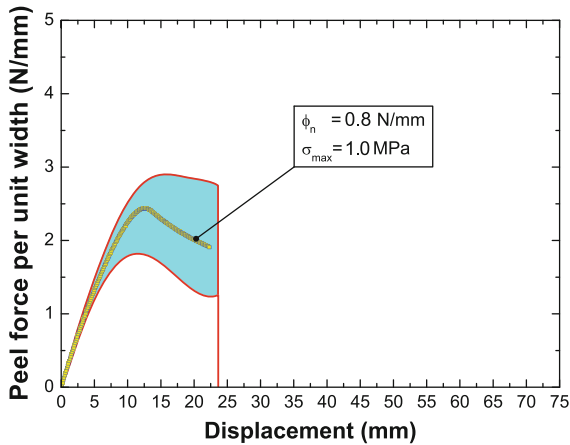
Fig. 8 Comparison between experiments and simulations for samples with grit blasted surfaces. The *shaded area* represents the range of the experimental results
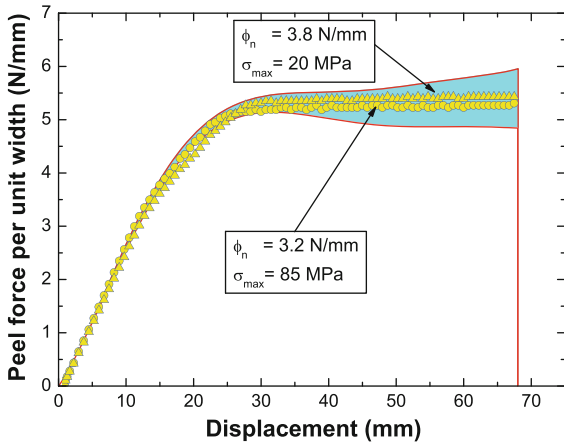
Fig. 9 Comparison between experiments and simulations for samples with laser treated surfaces. The *shaded area* represents the range of the experimental results

the above discussion, we may conclude that the bond toughness is up to four time greater than that recorded on samples with grit-blasted substrates. However, it is apparent that the determination of the full set of cohesive properties would require alternative procedures other than those based on global experimental data. Future works will focus on this matter.

References

Adams RD, Comyn J, Wake WC (1997) Structural adhesives joints in engineering. Chapman and Hall, London

Alfano G (2006) On the influence of the shape of the interface law on the application of cohesive-zone models. Compos Sci Technol 66(6):723–730

Alfano M (2010) Technical report. King Abdullah University of Science and Technology

Alfano M, Furgiuele F, Leonardi A, Maletta C, Paulino GH (2009) Mode I fracture of adhesive joints using tailored cohesive zone models. Int J Fract 157:193–204

Alfano M, Ambrogio G, Crea F, Filice L, Furgiuele F (2011a) Influence of laser surface modification on bonding strength of Al/Mg adhesive joints. J Adhes Sci Technol 25(11):1261–1276

Alfano M, Ambrogio G, Filice L, Furgiuele F, Gallus E, D'Antuoni D (2011b) On the performance of welded, riveted and adhesive bonded Al/Mg sheet metal joints. Key Eng Mater 473:237–242

Alfano M, Furgiuele F, Lubineau G, Paulino GH (2011c) Simulation of debonding in Al/epoxy T-peel joints using a potential based cohesive zone model. Proc Eng 10:1764–1769

Alfano M, Furgiuele F, Pagnotta L, Paulino GH (2011d) Analysis of fracture in aluminum joints bonded with a bi-component epoxy adhesive. J Test Eval 39(2):JTE102753

Alfano M, Furgiuele F, Lubineau G, Paulino GH. Study on the role of laser surface irradiation on damage and decohesion of Al/epoxy bonded joints. J Publ (submitted)

ASTM D1876-08 (2008) Standard test method for peel resistance of adhesives (T-Peel Test)

Baburaj EG, Starikov D, Evans J, Shafeev GA, Bensaoula A (2007) Enhancement of adhesive joint strength by laser surface modification. Int J Adhes Adhes 27(4):268–276

Baldan A (2004) Adhesively-bonded joints and repairs in metallic alloys, polymers and composite materials: adhesives, adhesion theories and surface pretreatment. J Mater Sci 39(1):1–49

Barenblatt GI (1962) Mathematical theory of equilibrium cracks in brittle fracture. Adv Appl Mech 7:55–129

Belcher MA, Wohl CJ, Connel JW (2010) Laser surface preparation and bonding of aerospace structural composites. In: Proceedings of the SAMPE symposium and exhibition

Cavalli MN, Thouless MD (2001) The effect of damage nucleation on the toughness of an adhesive joint. J Adhes 76(1):75–92

Dugdale DS (1960) Yielding steel sheets containing slits. J Mech Phys Solids 8(2):100–104

Fedele R, Raka B, Hild F, Roux S (2009) Identification of adhesive properties in GLARE assemblies using digital image correlation. J Mech Phys Solids 57:1003–1016

Gustafson PA, Waas AM (2009) The influence of adhesive constitutive paramaters in cohesive finite element models of adhesively bonded joints. Int J Solids Struct 46:2201–2215

Högberg JL (2006) Mixed mode cohesive models. Int J Fract 141:549–559

Ji G, Ouyang Z, Li G, Ibekwe S, Pang S-S (2010) Effect of adhesive thickness on global and local mode I interfacial fracture of bonded joints. Int J Solids Struct 47:2445–2458

Kafkalidis MS, Thouless MD, Yang QD, Ward SM (2000) Deformation and fracture of an adhesive layer constrained by plastically-deforming adherends. J Adhes Sci Technol 14(13):1593–1607

Kinloch AJ (1987) Adhesion and adhesives, science and technology. Chapman and Hall, London

Kinloch AJ, Lau CC, Williams JG (1994) The peeling of flexible laminates. Int J Fract 66:45–70

Lee MJ, Cho TM, Kim WS, Lee BC, Lee JJ (2010) Determination of cohesive paramaters for a mixed mode cohesive zone model. Int J Adhes Adhes 30:322–328

Loctite Hysol 9466 (2006) Technical data sheet

Man HC, Zhao NQ (2006) Enhancing the adhesive bonding strength of NiTi shape memory alloys by laser gas nitriding and selective etching. Appl Surf Sci 253:1595–1600

Park K, Paulino GH, Roesler JR (2009) A unified potential-based cohesive model of mixed-mode fracture. J Mech Phys Solids 57:891–908

Rechner R, Jansen I, Beyer E (2010) Influence on the strength and aging resistance of aluminum joints by laser pretreatment and surface modification. Int J Adhes Adhes 30(7):595–601

Shen B, Paulino GH (2011) Direct extraction of cohesive fracture properties from digital image correlation: a hybrid inverse technique. Exp Mech 51(2):143–161

Sun C, Thouless MD, Waas AM, Schroeder JA, Zavattieri PD (2008) Ductile-brittle tramsition in the fracture of plastically deforming adhesively bonded structures. Part II: numerical studies. Int J Solids Struct 45:4725–4738

Tvergaard V, Hutchinson J (1992) The relation between crack growth resistance and fracture process parameters in elasto-plastic solid. J Mech Phys Solids 40:1377–1397

Wei Y (2002) Thin layer splitting along the elastic-plastic solid surface. Int J Fract 113:233–252

Wei Y, Hutchinson JW (1998) Interface strenght, work of adhesion and plasticity in the peel tets. Int J Fract 93:315–333

Yang QD, Thouless MD (2001) Mixed mode fracture analyses of plastically deforming adhesive joints. Int J Fract 110:175–187

Yang QD, Thouless MD, Ward SM (1999) Numerical simulations of adhesively bonded beams failing with extensive plastic deformation. J Mech Phys Solids 47:1337–1353

Yang QD, Thouless MD, Ward SM (2000) Analysis of the symmetrical 90°-peel test with extensive plastic deformation. J Adhes 72(2):115–132

Yang QD, Thouless MD, Ward SM (2001) Elastic-plastic mode-II fracture of adhesive joints. Int J Solids Struct 38:3251–3262